Journal of Materials Chemistry A

Accepted Manuscript

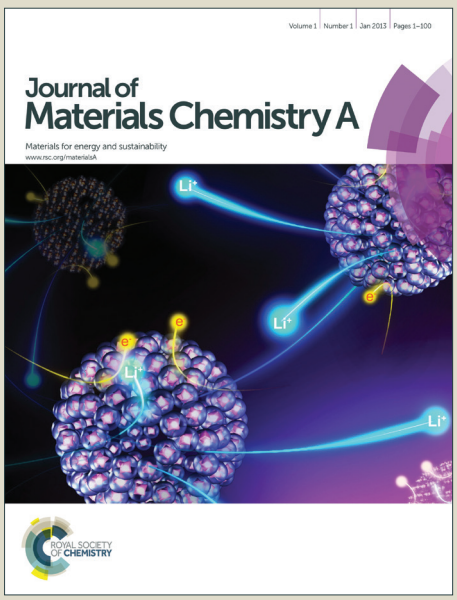

This is an *Accepted Manuscript*, which has been through the Royal Society of Chemistry peer review process and has been accepted for publication.

Accepted Manuscripts are published online shortly after acceptance, before technical editing, formatting and proof reading. Using this free service, authors can make their results available to the community, in citable form, before we publish the edited article. We will replace this *Accepted Manuscript* with the edited and formatted *Advance Article* as soon as it is available.

You can find more information about *Accepted Manuscripts* in the Information for Authors.

Please note that technical editing may introduce minor changes to the text and/or graphics, which may alter content. The journal's standard Terms & Conditions and the Ethical guidelines still apply. In no event shall the Royal Society of Chemistry be held responsible for any errors or omissions in this *Accepted Manuscript* or any consequences arising from the use of any information it contains.

ROYAL SOCIETY OF CHEMISTRY

www.rsc.org/materialsA

Controlled synthesis of pentachlorophenol-imprinted polymers on the surface of magnetic graphene oxide for highly selective adsorption

Sheng-Dong Pan[1,2], Hao-Yu Shen[3], Li-Xin Zhou[4], Xiao-Hong Chen[1,2], Yong-Gang Zhao[1,2], Mei-Qiang Cai[5], Mi-Cong Jin[1,2*]

([1]Zhejiang Provincial Key Laboratory of Health Risk Appraisal for Trace Toxic Chemicals, Ningbo Municipal Center for Disease Control and Prevention, Ningbo, Zhejiang, 315010, China; [2] Ningbo Key Laboratory of Poison Research and Control, Ningbo Municipal Center for Disease Control and Prevention, Ningbo 315010, China; [3] Ningbo Institute of Technology, Zhejiang Univercity, Ningbo, Zhejiang 315100, China; [4] Medical School, Ningbo University, Ningbo, Zhejiang, 315211, China; [5]School of Environmental Science and Engineering, Zhejiang Gongshang University, Hangzhou 310018)

Abstract: A novel well-designed magnetic graphene oxide sheet embedded with core-shell molecularly imprinted polymer microspheres (MGO@MIP) was controlledly synthesized via reflux-precipitation polymerization and surface imprinting technique. The as-prepared MGO@MIP was fully characterized and the obtained results revealed that the specific selectivity and remarkable adsorption capacity to pentachlorophenol (PCP) were closely relied on the synergetic effect of hydrogen bonds and π-π interaction, which are strongly related to the solution pH and the distribution of magnetic microspheres on the surface of GO sheet. Under the optimal conditions, *i.e.*, pH of 4.0 and the ratio of the usage amount of monomers to

*Corresponding author. E-mail address: jmcjc@163.com (M. C. Jin)

Journal of Materials Chemistry A Accepted Manuscript

Fe_3O_4 at 15, the maximum adsorption capacity and the imprinting factor (α) of MGO@MIP towards PCP were 789.4 mg/g and 4.36, respectively. The newly synthesized MGO@MIP was proved to be a great adsorbent for PCP in the environmental water.

1. Introduction

The wide use of pentachlorophenol (PCP) as disinfectants, pesticides, wood preservatives and pulp bleaching agents [1], leads to the inevitable emission and immission into the aquatic environment. Because of its high toxicity and unpleasant organoleptic properties, PCP has been included in the list of priority pollutants by the US Environmental Protection Agency (EPA) [2]. Obviously, the research and development of effective and selective methods to removal and separate PCP in environmental water samples has aroused great interest.

Until now, various treatment approaches for PCP removal have been developed, mainly including advanced oxidation [3], electrochemical oxidation [4], photocatalytic degradation [5], biological degradation [6], mechanochemical degradation [7] and adsorption [8-13]. Among these methods, the adsorption approach is considered as a promising method since it can effectively remove pollutants from the contaminated system by the convenient design and operation. Many adsorbents such as chitosans [8], organoclays [9], polymers [10, 11], and carbon nanotube [12] have been used to remove PCP. However, some of them show low adsorption capacity or poor selectivity. Graphene (G) has attracted great attention of researchers recent years due to its unique structure and extraordinary properties [13]. Notably, the large

Journal of Materials Chemistry A Accepted Manuscript

delocalized π-electron system and ultrahigh specific surface area of G make it a promising candidate with strong affinity and high adsorption capacity for hydrophobic compounds and carbon-based ring structures [14-16]. For the limits of existing physical approaches of G, chemical modification and functionalization has been focused on [17-19]. Recently, molecular imprinting technology has already been a highly accepted tool for the synthesis of tailor-made recognition materials with cavities that can selectively recognize target molecules [20, 21]. However, molecularly imprinted polymers (MIP) prepared via conventional technique have some disadvantages such as complex preparation and poor adsorption capacity. G, as a new supporter for MIP, has been developed to overcome these drawbacks because of its large specific surface area and high porosity 3D platform [22]. The MIP modified G makes it possible to enhance the selectivity and improve the binding kinetic properties, as well as the adsorption capacity towards target molecules. Li *et al.* [23] synthesized a molecularly imprinted polymer-graphene oxide (GO-MIP) hybrid material by reversible addition and fragmentation chain transfer (RAFT) polymerization using RAFT agent functionalized GO as chain transfer agent. The resulting GO-MIP hybrids showed outstanding affinity and appreciable selectivity towards 2,4-dichlorophenol (2,4-DCP) in aqueous solution. While Luo and his co-workers [24] developed a novel chitosan/graphene oxide-molecularly imprinted polymer (CGO-MIP) for recognition and determination of sulfamethoxazole (SMZ) based on a flow injection chemiluminescence (FI-CL). Despite the successful design of the proposed approach, difficulty for rapid separation after treatment from solution

Journal of Materials Chemistry A Accepted Manuscript

has limited their applications.

Recently, new separation methods based on magnetic nanomaterials have been proven to be simple, convenient, and powerful for the separation and purification of environmental samples, and removal of toxic pollutants in water [25-30]. In general, the success of this method is attributed to the fact that the magnetic materials possess unique magnetic properties and can be separated simply from the solution by a magnetic field. It was conceivable that, if three promising concepts (G, molecular imprinting, and magnetic separation) were combined in one system, a novel G-based magnetic MIP could be constructed with multifunctional performance, which has not only the selectivity and high adsorption capacity for the target molecule, but also the magnetic response ability.

Herein, we reported a successful method for the design and synthesis of a novel planar-structure G-based magnetic MIP (MGO@MIP), aiming at effective adsorption and recognition of PCP. The well-defined core-shell microspheres, consisting of a Fe_3O_4 nanoparticle core and an outer layer of polymer shell, were controlledly synthesized and then covalently bonded to GO sheet via reflux-precipitation polymerization and surface imprinting technique. The three-in-one system not only provides MIP with high adsorption capacity but also improves the selectivity of GO sheet for the target analytes. Meanwhile, the superparamagnetism of the incorporated Fe_3O_4 nanoparticles allows magnetic separation to replace the centrifugation and filtration steps.

2. Experimental

Journal of Materials Chemistry A Accepted Manuscript

2.1. Materials

Iron (III) chloride hexahydrate ($FeCl_3 \cdot 6H_2O$), sodium acetate anhydrous (NaAc), ethylene glycol (EG), sodium hydroxide (NaOH), and hydrochloric acid (HCl) were analytical grade, and purchased from Sinopharm Chemical Reagent Co., Ltd. (Shanghai, China). Divinylbenzene (DVB, purity>99%), glycidylmethacrylate (GMA, purity>99%), and ethanediamine (EDA, purity>99%) were supplied by Alddin Chemical Reagent Co., Ltd. (Shanghai, China) and purified by vacuum distillation. 2,2-azobis (2-methyl-propionitrile) (AIBN, purity>99%) was purchased from J&K Chemical (99%) and used as an initiator without further purification. Analytical grade of N-ethyl-N′-(3-(dimethylamino) propyl) carbodiimide (EDC) and N-hydroxysuccinimide (NHS) were obtained from TCI Tokyo Chemical Industry Co., Ltd (Tokyo, Japan). 2-chlorophenol (2-CP, purity>99%), 2,4-dichlorophenol (2,4-DCP, purity>99%), 2,3,4,6-tetrachloropyridine (2,3,4,6-TeCP, purity>99%) and pentachlorophenol (PCP, purity>99%) were supplied by Aladdin Chemical Reagent Co., Ltd. (Shanghai, China). HPLC grade of methanol, acetonitrile, formic acid and ammonium acetate (NH_4Ac) were obtained from Merck (Darmstadt, Germany).

2.2. Preparation of MGO@MIP

The overall preparation of PCP-imprinted polymer surface modified magnetic graphene oxide (MGO@MIP) is depicted in Scheme 1. The developed method exhibited facility, controllable and stable.

<Insert Scheme 1 >

2.2.1. Synthesis of magnetic Fe_3O_4

Journal of Materials Chemistry A Accepted Manuscript

The magnetic Fe_3O_4 was synthesized by solvothermal method according to the literature with a minor modification [31]. Briefly, $FeCl_3 \cdot 6H_2O$ (3.0 g) was dissolved in EG (80 g) to form a clear solution, followed by the addition of NaAc (6.7 g) and polyethylene glycol (2.0 g). The mixture was stirred vigorously for 30 min at 50 ^oC and then transferred to a teflon-lined stainless-steel autoclave (100 mL capacity). The autoclave was heated to and maintained at 200 ^oC for 6 h and then naturally cooled to room temperature. The black magnetic Fe_3O_4 particles were obtained and washed three times with methanol under ultrasonic conditions to remove the adsorbed solvent.

2.2.2. Controlled synthesis of MGO@MIP

Synthesis of core-shell magnetic Fe_3O_4@P(GMA-*co*-DVB) (Solution 1): Briefly, 80 mg of Fe_3O_4 inorganic seeds was suspended in 100 mL of acetonitrile solution containing DVB, GMA, and AIBN. Then the above suspension was placed in a 150 mL three-neck flask equipped with a mechanical stirrer, a thermometer with a temperature controller, a Graham condenser and a heating mantle. The reaction mixture was heated from ambient temperature until the boiling state, and the polymerization was further carried out under refluxing state for 2 h. After polymerization, the resultant Fe_3O_4@P(GMA-*co*-DVB) core-shell microspheres were washed three times with methanol and then dispersed in 50 mL morphine ethanesulfonic acid (MES, 0.1 mol/L, pH=5.6) buffer solution under ultrasound.

The core-shell magnetic polymer microspheres of Fe_3O_4@P(GMA-*co*-DVB)-1, Fe_3O_4@P(GMA-*co*-DVB)-2, and Fe_3O_4@P(GMA-*co*-DVB)-3 refer to the materials with the ratios of the usage amount of monomers (GMA+DVB, GMA:DVB=1:1) to

Journal of Materials Chemistry A Accepted Manuscript

Fe_3O_4 at 2.5, 15 and 28, respectively, during the polymerization process.

Activation of carboxyl groups on GO sheet (Solution 2): Firstly, 50 mg of GO in 10 mL MES buffer was ultrasonicated for 3 h, and then 9.6 mg of EDC and 5.8 mg of NHS were added into the suspension of GO and further ultrasonicated for 1 h to activated carboxyl groups of GO at room temperature.

Preparation of PCP template molecule solution (Solution 3): The template molecules (PCP, 2.0 mmol/L) and active groups (EDA, 200 mmol/L) were mixed and dissolved adequately in 50 mL MES buffer solution (0.1 mol/L pH=5.6). The self-assembling process took place via hydrogen-bonding interactions by stirring at 50 ^{o}C for 1 h.

Controlled synthesis of MGO@MIP: Afterward, the above three solutions were mixed and stirred vigorously at 80 ^{o}C under ultrasound. The PCP template molecules were grafted onto the material via ring-opening reaction and π-π stacking interaction. Finally, the template molecules were eluted with acetic acid/methanol (4:6, v/v) for several times under ultrasound until PCP could not be detected by HPLC. The as-prepared MGO@MIP were washed with water three times and dried at 60 ^{o}C.

The adsorbents of MGO@MIP-1, MGO@MIP-2, and MGO@MIP-3 were synthesized from Fe_3O_4@P(GMA-*co*-DVB)-1, Fe_3O_4@P(GMA-*co*-DVB)-2, and Fe_3O_4@P(GMA-*co*-DVB)-3, respectively.

In parallel, the non-imprinted polymer surface modified magnetic graphene oxide (MGO@NIP) was synthesized almost the same procedures described above but without the addition of the template molecules.

Journal of Materials Chemistry A Accepted Manuscript

Journal of Materials Chemistry A Accepted Manuscript

2.3. Characterizations

Scanning electron microscopy (SEM) was performed using scanning electron microscopy (SEM, JSM-6700F) at an accelerating voltage of 5.0 kV. Sample dispersed at an appropriate concentration in ethanol was cast onto a silicon sheet at room temperature and sputter-coated with gold.

Transmission electron microscopy (TEM) images were obtained on a Hitachi H-7650 transmission electron microscopy (TEM) (Hitachi, Japan) at an accelerating voltage of 75 kV. All the size data reflect the averages of about 100 particles and are calculated according to Eq. (1)[32]:

$$U = D_w / D_n, \quad D_n = \sum_{i=1}^{k} n_i D_i / \sum_{i=1}^{k} n_i, \quad D_w = \sum_{i=1}^{k} n_i D_{i_i}^4 / \sum_{i=1}^{k} n_i D_i^3 \quad (1)$$

where U is the polydispersity index, D_n is the number-average diameter, D_w is the weight-average diameter, and D_i is the diameter of the determined microspheres. The thickness of the shell layer is calculated to be half of the difference between the average diameter of the core-shell particles and that of the cores.

The magnetic properties of magnetic particles were measured using a vibrating sample magnetometer (VSM, Lake Shore 7410). Powder X-ray diffraction (XRD) patterns were collected on an X-ray diffractometer (Bruker D8 Advance) with CuKα radiation at λ= 0.154 nm operating at 40 kV and 40 mA.

Fourier Transform Infrared spectrometer (FTIR, Thermo Nicolet, USA), and X-ray photoelectron spectroscopy (XPS, AXIS ULTRADLD) were used to investigate the adsorption mechanism of PCP onto MGO@MIP. The fluorescence properties of MGO@MIP, PCP, and MGO@MIP-PCP (after adsorption) were

measured on a fluorescence spectroscopy (Hitach F4500). 50.0 mg of each solid sample were immobilized on a sample holder and measured by emission scan at 300 nm of fixed excitation wavelength.

2.4. HPLC analysis

HPLC analysis was performed on a Waters 2695 HPLC system including a binary pump and a UV detector (Waters Corporation, USA), using a ZORBAX SB-C18 (5 μm particle size, 150 mm×4.6mm) analytical column. The mobile phase was using methanol (A) and 0.1% (v/v) formic acid (B) at 1.0 mL/min. The linear gradient elution program was as follows: 0 min to 2.0 min, 40.0% to 70.0% (A); 2.0 min to 5.0 min, 70.0% to 95.0% (A); 5.0 min to 6.0 min, 95.0% to 40.0%; and 6.0 min to 10.0 min, 40.0% (A). The linear gradient of detection wavelength was as follows: 0 min to 6.5 min, 280 nm; 6.6 min to 8.0 min, 304 nm; and 9.0 min to 10.0 min, 280 nm. Column was maintained at a temperature of 35 °C to enhance the retention time reproducibility, and the injection volume was 10.0 μL.

2.5. Adsorption experiments

Batch adsorption experiments were carried out in 150 mL stoppered flasks, and each of them contained 40 mL of PCP solution. The solution pH was adjusted by 0.1 mol/L HCl or 0.1 mol/L NaOH, and then 20 mg of adsorbents were added into each flask and shaken at 180 rpm in a thermostatic shaker. The PCP concentration in the supernatant was measured by HPLC. According to the PCP concentrations before and after adsorption, the equilibrium adsorption capacity (q, mg/g) of PCP bound to the MGO@MIP is calculated using Eq. (2):

Journal of Materials Chemistry A Accepted Manuscript

$$q = \frac{(C_0 - C_e)V}{m} \qquad (2)$$

where C_0 and C_e represent the initial solution concentration and the equilibrium concentration of PCP (mg/L), V is the volume of the PCP solution (mL), m is the adsorbent dosage (mg), the same hereinafter.

To investigate the effect of pH, 40 mL of 100 mg/L PCP with pH ranging from 2.0 to 9.0 were mixed with 20 mg of magnetic adsorbents for 1 h at 308 K, respectively. In the kinetic experiments, the MGO/MIP was also investigated with contacting time ranging from 1 to 180 min at pH 4.0. The pseudo-second-order model (Eq. (3)) [33] were used to fit the experimental data.

$$\frac{t}{q_t} = \frac{1}{k_2 q_e^2} + (\frac{1}{q_e})t \qquad (3)$$

where q_t is the adsorption capacity at time t (mg/g), k_1 (min^{-1}), k_2 (g/(mg·min) are the adsorption rate constants.

The adsorption isotherm studies were investigated with PCP initial concentration ranging from 10 to 1000 mg/L, under pH 4.0 at 308 K for 1 h. Freundlich model (Eq. (4)) was applied to analyze the adsorption data.

$$\log q_e = \log K_F + \frac{1}{n}\log C_e \qquad (4)$$

where K_F is a Freundlich constant related to adsorption capacity and $1/n$ is a Freundlich constant related to the adsorption intensity.

Three kinds of MGO@MIP with different polymer shell thickness were used to investigate the effect of polymer shell on the PCP removal at initial PCP concentration of 100 mg/L.

2.5. Selectivity

Journal of Materials Chemistry A Accepted Manuscript

Analogs of PCP, including 2-CP, 2,4-DCP, and 2,3,4,6-TeCP were chosen to evaluate the selectivity of the MGO@MIP and MGO@NIP and individually dispersed into 40 mL of 100 mg/L PCP. The mixtures were shaken for 1 h at 308 K, and the concentrations of PCP and the analogs in the supernatants were analyzed by HPLC. The binding amounts of PCP and the analogs to MGO@MIP and MGO@NIP were then compared.

3. Results and discussion

3.1. Synthesis and characterization of MGO@MIP

This work focused on controlled synthesis of PCP-imprinted MGO@MIP via reflux precipitation polymerization, molecules self-assembly coupled with grafting reaction. Under optimized parameters, the resulting materials can exhibit a homogeneous morphology, highly selective recognition, strong affinity ability, and high magnetic responsiveness for the adsorption of PCP from environmental water samples.

Magnetic Fe_3O_4 microspheres were prepared through a solvothermal method according to the literature with a minor modification by partial reduction of $FeCl_3$ with EG as solvent, NaAc as an alkali source, and PEG as a stabilizer at 200 ^{o}C. The Fe_3O_4 microspheres had a spherical shape with a rough surface, which could help to be further coated by polymers, and relative uniform size around 300 nm (Fig. 1a and b). As can be seen in Fig. 2a, the magnetic response of Fe_3O_4 synthesized by solvothermal method is higher (86 emu/g) than that by coprecipitation method (65.6 emu/g) [34], which indicates the Fe_3O_4 prepared by solvothermal method is easier to

Journal of Materials Chemistry A Accepted Manuscript

be separated by external magnetic field.

Reflux-precipitation polymerization is a newly developed method by Wang *et al.* [35]. Similar to precipitation polymerization, it consists of three components, *i.e.*, monomer, initiator and organic solvent, without the addition of any surfactants or stabilizers. Compared to common precipitation polymerization, reflux-precipitation polymerization is a wide spectrum of functional monomers. In this work, the effect of different amounts of monomers (GMA and DVB) was investigated. It can be seen from Fig. 1 c, d, and e that the uniform polymeric shell of lower image contrast surrounding the inorganic Fe_3O_4 core was easily discernible. The grey polymer shells of different thicknesses could be obtained via adjusting the initial amount of monomers during reflux-precipitation polymerization. The size, size distribution, and shell thickness of the obtained core-shell Fe_3O_4@P(GMA-*co*-DVB) microspheres were listed in Table 1. It indicates that the shell thickness increased with the amount of monomer increasing, while the monodispersity decreased. In the polymerization process, DVB was selected as a cross-linking agent because of its faster reaction rate and better hydrophilicity compared to GMA, making GMA inclined to the outside surface of the microspheres in acetonitrile [36]. Thus, the reactive epoxy groups of GMA could be easily reacted with self-assembled EDA-PCP via opening-reaction. In this stage, the template molecules (PCP) were fabricated onto magnetic graphene oxide via hydrogen bond and π-π stacking interaction, and the final PCP-imprinted MGO@MIP could be obtained by eluting the template molecules with acetic acid/methanol (4:6, v/v) for several times under ultrasound. The TEM image of

Journal of Materials Chemistry A Accepted Manuscript

MGO@MIP was exhibited in Fig. 1f, in which core-shell magnetic polymer microspheres were covalently bonded on the surface of GO.

<Insert Table 1>

The magnetic properties of Fe_3O_4@P(GMA-*co*-DVB) microspheres with different shell thicknesses were measured by VSM at room temperature (Fig. 2 a). After coating with polymer layer of P(GMA-*co*-DVB), the magnetization values dramatically decreased from 86.43 (Fig. 2a(i)) to 46.81 (Fig. 2a(ii)) and 4.62 emu/g (Fig. 2a(iv)) with the increase of polymer component.

To further demonstrate the crystal structure of MGO@MIP, the XRD patterns of the as-prepared Fe_3O_4, MGO@MIP and GO were collected (Fig. 2b). As shown in Fig. 2b(i), the position and relative intensities of all diffraction peaks at 2θ=30.25^o, 35.58^o, 43.21^o, 54.39^o, 57.09^o, and 62.92^o can be assigned to (220), (311), (400), (422), (511) and (440) reflections, respectively, confirming the pure cubic spinel crystal structure of Fe_3O_4. Fig.2b(ii) presents a sharp diffraction peak at 2θ=11.28^o, which can be assigned to the (002) reflection of layer GO [37]. As for MGO@MIP (Fig. 2b(iii)), six characteristic peaks for Fe_3O_4 appeared while the (002) reflection peak of GO can not be observed. This could be owing to the fact that the GO sheets can not stack with each other any more to form crystalline structures after covering with magnetic polymer microspheres [38].

<Insert Fig. 1 and Fig. 2>

3.2 Binding characteristics of MGO@MIP

3.2.1 Effect of pH and adsorption mechanism

Journal of Materials Chemistry A Accepted Manuscript

The effect of solution pH was investigated with the pH values ranging from 2.0 to 9.0, and the results showed that the adsorption capacity of PCP was highly dependent on solution pH (Fig.3). Moreover, 4.0 was the optimal pH value for PCP adsorption, at which the adsorption amounts were 196.2 and 73.6 mg/g for MGO@MIP and MGO@NIP, respectively. With the solution pH increasing, the adsorption capacities firstly increased gradually with the solution pH ranging from 2.0 to 4.0, and sharply decreased with the pH in range of 4.0 to 7.0, and reached a plateau value with pH ranging from 7.0 to 9.0. The higher adsorption capacity of MGO@MIP than MGO@NIP was owing to the large number of active sites on the surface imprinting cavities.

The dependence of PCP adsorption on solution pH could be explained from the perspectives of surface charge of the adsorbent and the state of PCP at various pH values. In the present work, the state of PCP (pKa=4.7) and amino groups on MGO@MIP is significantly affected by solution pH. When pH<pKa, the amino groups are easy to protonate, and the main formation was $–NH_3^+$, which doesn't have lone pair electrons and it was difficult to form hydrogen bond (-O-H···N) with PCP. Thus, the adsorption capacity was worse compared to that of pH=4.0, at which the main formation of the surface groups might be $–NH_2$ and it was beneficial to form hydrogen bond (-O-H···N). Meanwhile, when pH>pKa, most of the PCP molecules presented in an ionic state (deprotonation of hydroxyl group), which resulted in difficulties to form hydrogen bonds (-O-H···N) with amino groups on the surface of MGO@MIP. It was worth concerning that the adsorption capacities of PCP under

Journal of Materials Chemistry A Accepted Manuscript

acidic conditions (pH<4.0) were higher than that of pH>4.0. This could also be explained from the perspectives of the charge of PCP and the state of the adsorbent. The scheme of adsorption mechanism was shown in Fig. 4. Under acidic conditions (pH<4.0), $–NH_3^+$ was difficult to form hydrogen bond with PCP by -O-H···N, while -C=O also could easily form hydrogen bond with molecular state of PCP (-C=O···H), as well as the hydrogen bond -N-H···Cl [39, 40], -N-H···O and π-π interaction with GO sheets (Fig. 4a). However, the main driving forces for PCP adsorption were only the hydrogen bond -N-H···Cl and π-π interaction when pH>4.0 (Fig. 4c), resulting in the worst adsorption capacity. When the pH=4.0, the above five driving forces, including -O-H···N, -C=O···H, -N-H···Cl, -N-H···O and π-π interaction with GO sheets, were coexisted to obtain the highest adsorption capacity of PCP (Fig. 4b).

<Insert Fig. 3 and Fig. 4>

The adsorption mechanism could be confirmed by XPS, FTIR, and fluorescence spectroscopy of MGO@MIP before and after PCP adsorption (Fig. 5). From the survey scan of XPS spectra (Fig. 5a), a new peak owing to Cl2p could be observed after PCP loaded on MGO@MIP, indicating the successful adsorption of PCP. The N1s high-resolution scan of MGO@MIP could be deconvoluted into two individual peaks at binding energies of 398.9 eV and 396.6 eV (Fig. 5b), which were assigned to C-N, and N-H [41], respectively. Two new peaks at 399.7 eV and 397.7 eV was observed after PCP adsorption, which could be attributed to the hydrogen bonding of

Journal of Materials Chemistry A Accepted Manuscript

ph-O-H···N, and -N-H···O-ph (or -N-H···Cl-ph), respectively. The C1s high-resolution scan of MGO@MIP could be fitted into three peaks (Fig. 5c) at 286.0 eV, 284.3 eV, and 282.3 eV, which could be attributed to C=O, C-N, and C-C (C-H), respectively [42]. After PCP adsorption, the intensity of C-N (284.3 eV) got much weaker compared to that of MGO@MIP, and a new peak with binding energy of 284.7 eV arose, which could be assigned to the hydrogen bonding of –C-N···H-O-ph between MGO@MIP and PCP. The O1s high-resolution scan of MGO@MIP could be fitted into two peaks (Fig. 5d) with binding energies of 530.1 eV and 529.1 eV, which were attributed to ether oxygen (C-O) and ester oxygen (O-C=O), respectively. A new weak binding energy peak at 530.1 eV was observed after PCP loaded, which could be attributed to the binding energy of ph-O in PCP.

In the FTIR spectra of MGO@MIP (Fig. 5e), the characteristic peak of Fe_3O_4 occurs at ~589 cm^{-1}. Other typical peaks could be assigned as follows, v(-OH): ~3402 cm^{-1}; v(-CH_2, -CH_3): ~2923 cm^{-1}, 2854 cm^{-1}; v(-C=O): ~1728 cm^{-1}; δ (-CONH-): ~1633 cm^{-1}; δ(N-H): ~1566 cm^{-1}. These revealed that the magnetic Fe_3O_4 was coated by the polymer and the core-shell Fe_3O_4@P(GMA-*co*-DVB) microspheres were successfully bonded onto the GO sheet via amide bond. From Fig. 5e, it also can be seen that a new peak located at ~721.4 cm^{-1} can be clearly observed after PCP loaded on MGO@MIP, which was attributed to the stretching vibration of C-Cl bond [43]. This suggests that PCP has been successfully adsorbed on MGO@MIP. Moreover, the peak of N-H bond at ~1566 cm^{-1} shifted to ~1533 cm^{-1}, indicating that the hydrogen bonds (-N-H···O and -N-H···Cl) were formed between PCP and –NH_2 groups

Journal of Materials Chemistry A Accepted Manuscript

provided by MGO@MIP [44]. Additionally, the peak of -C=O at ~1728 cm^{-1} shifted to ~1723 cm^{-1},which should be assigned to the hydrogen bond between C=O and PCP (C=O···H-O-ph). It was worth concerning that the peaks at ~1459 cm^{-1} and ~1390 cm^{-1}, owing to the skeletal vibration of aromatic C=C bonds, were shifted to ~1433 cm^{-1} and ~1367 cm^{-1}, suggesting the π-π stacking interaction might be formed between benzene ring of PCP and the hexagonal skeleton of GO sheet on the MGO@MIP [45]. Furthermore, the π-π stacking interaction could also be confirmed by fluorescence spectroscopy. As shown in Fig. 5f, the fluorescence intensities of MGO@MIP were quenched a lot after PCP adsorbed, implying the π-π stacking interaction appeared between PCP and MGO@MIP [46]. It was worthwhile to note that the degree of fluorescence-quenching increased with the increase of PCP amount loading onto MGO@MIP. Therefore, the adsorption mechanisms concluded from the batch adsorption data could be perfectly confirmed by the XPS, FTIR, and fluorescence spectroscopy.

<Insert Fig. 5>

3.2.2 Kinetic studies and adsorption capacity

Fig. 6 presented the adsorption kinetics of PCP onto MGO@MIP and MGO@NIP. The adsorption capacity was increased with time increased and MGO@MIP exhibited a high adsorption rate. In the first 5 min, the adsorption rate was increased rapidly and reached equilibrium after 10 min. By contrast, the time required to achieve equilibrium for MGO@NIP was 60 min. Therefore, in our case, PCP could reach the surface imprinting cavities of MGO@MIP easily and took less time to get adsorption

Journal of Materials Chemistry A Accepted Manuscript

equilibrium, implying that the micro-nano sized, surface imprinting and uniform structures of MGO@MIP allowed efficient mass transport. Besides, the adsorption kinetic data could be well described by pseudo-second-order model (Table 2). Moreover, the kinetic curve of MGO@NIP in Fig. 6 could be divided into three portions, which could be described by intraparticle diffusion model. This indicated that the intraparticle process was one of the rate-limiting steps [47] for PCP removal by MGO@NIP, and indicated that many binding sites of the non-imprinting MGO@NIP were hidden inside the adsorbent. Unlike MGO@NIP, the kinetic curve of MGO@MIP could only be divided into two portions, thus, the intraparticle process was not be involved in the rate-limiting steps. This could be owing to that a large number of active sites on the surface imprinting cavities of MGO@MIP prepared by surface imprinting technique and the improvement of mass transfer result in faster diffusion from the solution into the binding sites.

< Insert Fig. 6 and Table 2>

The adsorption capacity of MGO@MIP and MGO@NIP were investigated by dispersing the adsorbents in PCP solutions with various concentrations in range of 10.0 mg/L to 1000.0 mg/L and shaking for 1 h. The supernatants were analyzed by HPLC after magnetic separation. The results indicated that the adsorption capacity of MGO@MIP was much higher than that of MGO@NIP, and the adsorption capacity of PCP increased linearly with the increase of initial concentration of PCP. Furthermore, the Freundlich isotherm could well describe the adsorption process for both MGO@MIP and MGO@NIP, with both R^2>0.999 (Table 3). Besides, MGO@MIP

Journal of Materials Chemistry A Accepted Manuscript

had larger K_F value (40.54) than that of MGO@NIP (21.32), implying higher adsorption capacity, intensity and affinity for PCP [48]. This could be contributed to the reason that surface imprinting technique enhanced the formation of large number of active sites on the surface imprinting cavities of MGO@MIP.

<Insert Table 3 >

3.2.3. The adjustment of polymer shell thickness on the adsorption efficiency

The polymer shell thickness would affect the adsorption capacity of MGO@MIP towards PCP because it would affect the distribution of polymer microspheres on the surface of GO sheet. The batch adsorption experiments were carried out at a initial PCP concentration of 100 mg/L by MGO@MIP with different polymer shell thicknesses named as MGO@MIP-1 (50 nm), MGO@MIP-2 (310 nm), and MGO@MIP-3 (520 nm). The results showed that MGO@MIP-2 with a moderate polymer shell thickness exhibited the highest adsorption capacity (178.6 mg/g) among the three adsorbents (The adsorption capacities of MGO@MIP-1 and MGO@MIP-3 were 68.3 mg/g and 132.5 mg/g, respectively). This could be confirmed from the characterization results of FTIR, and XPS (Fig. 7).

As shown in FTIR spectra (Fig. 7a), after PCP loaded onto MGO@MIP with different polymer shell thicknesses, the peak of N-H bond at ~1562 cm^{-1} shifted to ~1533 cm^{-1}, indicating that the hydrogen bonds (-N-H···O and -N-H···Cl) were formed between PCP and $–NH_2$ groups provided by MGO@MIP. While a new peak located at ~721.4 cm^{-1}, owing to the stretching vibration of C-Cl bond of PCP [43], could be clearly observed. It was worth that with the increase of polymer shell

Journal of Materials Chemistry A Accepted Manuscript

thickness, both two characteristic peaks (~1533 cm^{-1} and ~721 cm^{-1}) enhanced first and then weakened, suggesting that PCP adsorption efficiency was first increased and then decreased with the polymer shell thickness increasing, which was perfectly consistent with the adsorption data. This could be owing to the adjustment of core-shell magnetic polymer microspheres. When the polymer shell was too thin (50 nm), the low ratio of functional monomer (GMA) results in low content of loaded $–NH_2$ groups on the surface of MGO@MIP-1. Thus, the hydrogen bonds (-N-H···O, -N-H···Cl and -O-H···N) were limited. When the polymer shell was too thick (520 nm), the large size of Fe_3O_4@P(GMA-*co*-DVB)-3 would completely cover the surface of GO sheet and the contribution of GO sheet to the adsorption process would be hidden. The polymer shell thickness of MGO@MIP-2 (~310 nm) was optimal in this study. The space between neighbouring microspheres was suitable for PCP adsorption (Fig. 1f), which allowed better performances for both microspheres and GO sheet.

The same conclusion could also be obtained from Cl2p high-resolution spectra of the MGO@MIP after PCP adsorption (Fig. 7b). As shown in Fig. 7b, the peaks of $Cl2p_{1/2}$ and $Cl2p_{3/2}$ located at 197.9 eV and 199.4 eV could be assigned to the absorption of Cl on PCP [49], indicating the successfully binding of PCP onto MGO@MIP. Besides, with the thickness of polymer shell increased, the peaks of $Cl2p_{1/2,\ 3/2}$ first enhanced and then weakened, implying the adsorption efficiency of PCP onto MGO@MIP was obviously varying with the polymer shell thickness changing. This perfectly confirmed the conclusions of adsorption data and FTIR

Journal of Materials Chemistry A Accepted Manuscript

results.

<Insert Fig. 7>

3.2.4 Adsorption selectivity

Selective recognition towards the template molecule, which depends upon the imprinted cavities in imprinted materials to the size, shape, and functionality of the template molecule, is of importance for a novel imprinted material. Herein, the selectivities of MGO@MIP and MGO@NIP towards PCP and other three CPs (2-CP, 2,4-DCP, 2,3,4,6-TeCP) were studied. PCP was selected as referent to investigate the selectivity of the imprinted material. The imprinting factor (α) and selectivity factor (β) were used to estimate the specific recognition property of the imprinted material [50]. The imprinting factor was defined as Eq. (5):

$$\alpha = \frac{q_A}{q_B} \tag{5}$$

where q_A and q_B are the capacities of MIP and NIP to adsorb the template or referent. The selectivity factor is defined as Eq. (6):

$$\beta = \frac{\alpha_1}{\alpha_2} \tag{6}$$

where α_1 is the imprinting factor with respect to the template and α_2 is the imprinting factor with respect to the referent.

As shown in Fig. 8, the adsorption capacity of MGO@MIP to adsorb PCP was much greater than the capacity to adsorb 2-CP, 2,4-DCP and 2,3,4,6-TeCP compared to MGO@NIP. The imprinting factor (α) of MGO@MIP for PCP was 4.36, which was larger than those of the referents (Table 4). The high selectivity factors (β) of the

Journal of Materials Chemistry A Accepted Manuscript

referents were as listed in Table 4, which also exhibited the excellent selectivity of MGO@MIP toward PCP. This could be attributed to its specific binding sites.

<Insert Table 4 and Fig. 8>

3.3 Reuse experiments and comparison of adsorption properties

The reusable of the MGO@MIP was evaluated by comparing the adsorption capacity. The PCP loaded GO@MIP was extracted with methanol/ammonia (90:10, v/v) for 1 h after used, and then for adsorption to get the adsorption capacity. The results, as shown in Fig. 9, indicated that MGO@MIP could be used for ten cycles with a loss of less than 5.6% upon recovery on average. No obvious decrease in the adsorption capacity was found, implying that the MGO@MIP was stable and could be recycled.

<Insert Fig. 9>

The adsorption capacities of MGO@MIP and MGO@NIP compared with other adsorbents examined for the removal of PCP under similar conditions are summarized in Table 5. The results indicate that the as-prepared MGO@MIP in this work has a much higher adsorption capacity than those of other adsorbents reported in the literatures. Hence, the new developed MGO@MIP has promising potential applications in the removal of PCP from environmental water.

<Insert Table 5>

4. Conclusions

A novel PCP-imprinted MGO@MIP was controlledly prepared by reflux-precipitation polymerization and surface imprinting technique. The proposed

Journal of Materials Chemistry A Accepted Manuscript

method exhibited excellent controllability and the as-prepared MGO@MIP showed desirable levels of magnetic responsibility and chemical stability. Furthermore, PCP-imprinted MGO@MIP indicated high adsorption capacity, high selectivity, and rapid binding activity toward PCP. These results implied that the synthesized MGO@MIP could be used for separation and removal of PCP from environmental water samples.

Acknowledgements

We would like to thank the National Natural Science Foundation of China (No. 21377114), Ningbo Natural Science Foundation of China (No. 2013A610242, No. 2013A610243, No. 2014A610283 and No. 2014A610092), Zhejiang Provincial Natural Science Foundation of China (LY12H26003, LY14B070004 and LY14B040003), the Medical Health Foundation for Key Talents in Zhejiang Province, China (No.2013KYA187), the Constructive Major Project for the Department of Health and Family Planning Commission–Zhejiang Province (2014PYA019) and Zhejiang Provincial Program for the Cultivation of High-level Innovative Health Talents for their financial support of this research.

References

1. F. Galán-Cano, R. Lucena, S. Cárdenas and M. Valcárcel, *J. Chromatogra. A* 2012, 1229, 48-54.

2. Toxic Substance Control Act, U.S. Environmental Protection Agency, Washington, DC, 1979.

3. S. Esplugas, J. Giménez, S. Contreras, E. Pascual and M. Rodríguez, *Water Res.*

Journal of Materials Chemistry A Accepted Manuscript

2002, 36, 1034-1042.

4. J. Niu, Y. Bao, Y. Li and Z. Chai, *Chemosphere* 2013, 92, 1571-1577.

5. Y. Li, J. Niu, L. Yin, W. Wang, Y. Bao, J. Chen and Y. Duan, *J Environ Sci.* 2011, 23, 1911-1918.

6. L. Huang, L. Gan, Q. Zhao, B.E. Logan, H. Lu and G. Chen, *Bioresource Technol.* 2011, 102, 8762-8768.

7. P. Di Leo, M.D.R. Pizzigallo, V. Ancona, F. Di Benedetto, E. Mesto, E. Schingaro and G. Ventruti, *J. Hazard. Mater.* 2013, 244, 303-310.

8. S. Zheng, Z. Yang, D.H. Jo and Y.H. Park, *Water Res.* 2004, 38, 2314-2321.

9. Y. Park, G. A. Ayoko, E. Horvath, R. Kurdi, J. Kristof and R. L. Frost, *J. Colloid Interface Sci.*, 2013, 393, 319-334.

10. C. Păcurariu, G. Mihoc, A. Popa, S. G. Muntean and R. Ianoş, *Chem. Eng. J.,* 2013, 222, 218-227.

11. N. Li, Z. Mei and X. Wei, *Chem. Eng. J.,* 2012, 192, 138-145.

12. M.A. Salam and R.C. Burk, *Water, Air, Soil Poll., 2010,* 210, 101-111.

13. K. S. Novoselov, A. K. Geim, S. V. Morozov, D. Jiang, Y. Zhang and S. V. Dubonos, *Science*, 2004, 306, 666–669.

14. M. Hou, X. Zang, C. Wang and Z. Wang, *J. Sep. Sci.*, 2013, 36, 3242-3248.

15. Y. Yao, S. Miao, S. Liu, L. P. Ma, H. Sun and S. Wang, *Chem. Eng. J.*, 2012, 184, 326-332.

16. L. Ai, C. Zhang and Z. Chen. *J. Hazard. Mater.*, 2011, 192, 1515-1524.

17. S. Stankovich, D. A. Dikin, G. H. B. Dommett, K. M. Kohlhaas, E. J. Zimney and E. A. Stach, *Nature*, 2006, 442, 282-286.

Journal of Materials Chemistry A Accepted Manuscript

18. S. Park, J. H. An, R. D. Piner, I. Jung, D. X. Yang and A. Velamakanni, *Chem. Mater.*, 2008, 20, 6592-6594.

19. L. M. Veca, F. S. Lu, M. J. Meziani, L. Cao, P. Y. Zhang and G. Qi, *Chem. Commun.,* 2009, 2565-2567.

20. C. Xu, X. Shen and L. Ye, *J. Mater. Chem.*, 2012, 22, 7427-7433.

21. R. Gao, X. Kong, X. Wang, X. He, L. Chen and Y. Zhang, *J. Mater. Chem.*, 2011, 21, 17863-17871.

22. M. Yan, B. Yu, G. Shiyu, L. Fenghua and N. Li, *Biosens. Bioelectron*., 2011, 28, 291-297.

23. Y. Li, X. Li, C. Dong, J. Qi and X. Han. *Carbon*, 2010, 48, 3427-3433.

24. H. Qiu, L. Fan, X. Li, L. Li, M. Sun and C. Luo, *Carbohyd. Polym.*, 2013, 92, 394-399.

25. S. Pan, H. Shen, Q. Xu, J. Luo and M. Hu, *J. Colloid Interface Sci.,* 2012, 365, 204-212.

26. S. Pan, Y. Zhang, H. Shen and M. Hu, *Chem. Eng. J., 2012, 210, 564-574.*

27. Y. Li, C. Dong, J. Chu, J. Qi and X. Li, *Nanoscale*, 2011, 3, 280-287.

28. J. Liu, W. Wang, Y. Xie, Y. Huang,Y. Liu, X. Liu, R. Zhao, G. Liu and Y. Chen, *J. Mater. Chem.*, 2011, 21, 9232-9238.

29. M. Zhao, C, Zhang, Y. Zhang, X. Guo, H. Yan and H. Zhang, *Chem. Commun.,* 2014, 50, 2208-2210.

30. X. Xia, Edward P. C. Lai and B. Örmeci, *Environ. Sci. Pollut. Res.*, 2013, 20, 3331-3339.

31. H. Deng, X. Li, Q. Peng, X. Wang, J. Chen and Y. Li, *Angewandte Chemie*, 2005, 117, 2842-2845.

32. B. Liu, W. Zhang, F. Yang, H. Feng and X. Yang, *J. Phys. Chem. C*, 2011, 115, 15875-15884.

33. Y.S. Ho and G. Mckay, *Process Biochem*., 1999, 34, 451-465.

Journal of Materials Chemistry A Accepted Manuscript

34. B. Feng, R. Y. Hong, L. S.Wang, L. Guo, H. Z. Li, J. Ding, Y. Zheng and D. G.Wei, *Colloids and Surfaces A: Physicochem. Eng. Aspects*, 2008, 328, 52-59.

35. F. Wang, Y. Zhang, P. Yang, S. Jin, M. Yu, J. Guo and C. Wang, *J. Mater. Chem. B*, 2014, 2, 2575-2582.

36. J. M. Jin, J. M. Lee, M. H. Ha, K. Lee and S. Choe, *Polymer*, 2007, 48, 3107-3115.

37. A. V. Murugan, T. Muraliganth, A. Manthiram, *Chem. Mater.*, 2009, 21, 5004-5006.

38. H. K. He and C. Gao, *ACS Appl. Mater. Interfaces*, 2010, 2, 3201-3210.

39. Christopher J. Adams, Alessandro Angeloni, A. Guy Orpen, Thomas J. Podesta and Benjamin Shore, *Cryst. Growth Des.,* 2006, 6, 411-422.

40. D. Y. Wang, J. L. Wang, D. W. Zhang and Z. T. Li, *Sci. China Chem.*, 2012, 10, 2018-2026.

41. P. L. Lee, Y. K. Chui, Y. C. Sun and Y. C. Ling, *Carbon*, 2010, 48, 1397-1404.

42. Y. G. Zhao, X. H. Chen, S. D. Pan, H. Zhu, H. Y. Shen and M. C. Jin, *J. Mater. Chem. A*, 2013, 1, 11648-11658.

43. J. Chen, M. A. Hamon, H. Hu, Y. Chen, A. M. Rao, P. C. Eklund and R. C. Haddon, *Science*, 1998, 282, 95-98.

44. L. Zhou, L. Ji, P. C. Ma, Y. Shao, H. Zhang, W. Gao and Y. Li, *J. Hazard. Mater.*, 2014, 265, 104-114.

45. Y. Zhang, Y. Tang, S. Li and S. Yu, *Chem. Eng. J.*, 2013, 222, 94-100.

46. M. Liu, H. Zhao, S. Chen, H. Yu and X. Quan, *Environ. Sci. Technol.*, 2012, 46, 12567-12574.

47. A. Ramesh, H. Hasegawa, W. Sugimoto, T. Maki and K. Ueda, *Bioresour. Technol.*, 2008, 99, 3801-3809.

48. F.S. Zhang and H. Itoh, *J. Hazard. Mater. B*, 2003, 101, 323-337.

Journal of Materials Chemistry A Accepted Manuscript

49. P. Ji, G. Qu and J. Li, *Plasma Sci. Technol*., 2013, 15, 1059-1065.

50. W. Zhang, L. Qin, X.-W. He, W.-Y. Li and Y.-K. Zhang, *J. Chromatogr. A*, 2009, 1216, 4560-4567.

Journal of Materials Chemistry A Accepted Manuscript

Figures, Scheme and Tables

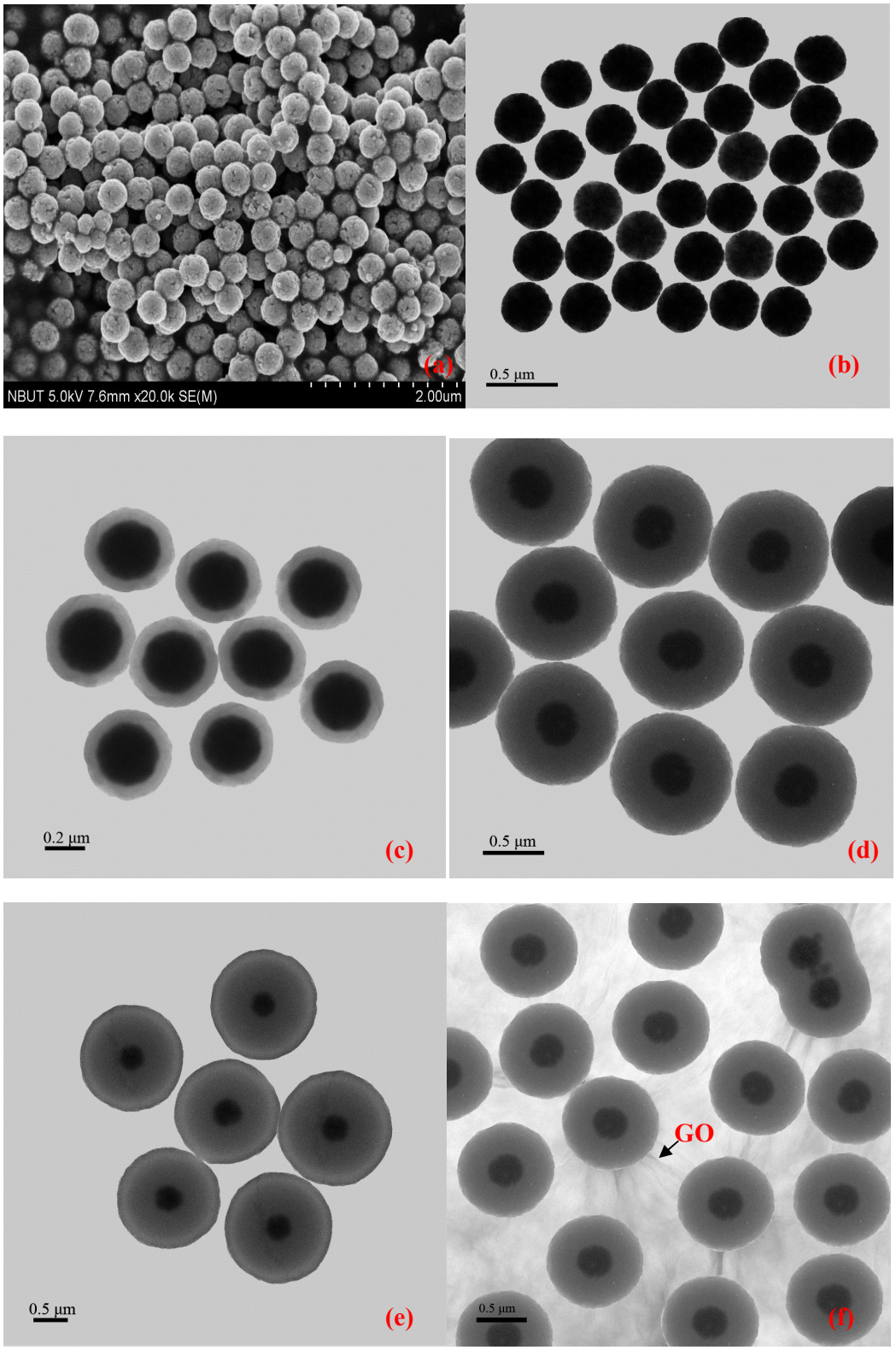

Fig. 1 (a) SEM image of Fe_3O_4 microsperes; (b) TEM image of Fe_3O_4 microsperes; (c), (d), (e)

Journal of Materials Chemistry A Accepted Manuscript

TEM images of core-shell structure Fe_3O_4@P(GMA-*co*-DVB) with different thickness of polymer shell named as Fe_3O_4@P(GMA-*co*-DVB)-1[a], Fe_3O_4@P(GMA-*co*-DVB)-2[a] and Fe_3O_4@P(GMA-*co*-DVB)-3[a], respectively ; (f) TEM image of MGO@MIP

[a] Fe_3O_4@P(GMA-*co*-DVB)-1, Fe_3O_4@P(GMA-*co*-DVB)-2, and Fe_3O_4@P(GMA-*co*-DVB)-3 mean the core-shell magnetic polymers with the ratio of the usage amount of monomers (GMA+DVB, GMA:DVB=1:1) to Fe_3O_4 at 2.5, 15 and 28, respectively, during the polymerization process.

Journal of Materials Chemistry A Accepted Manuscript

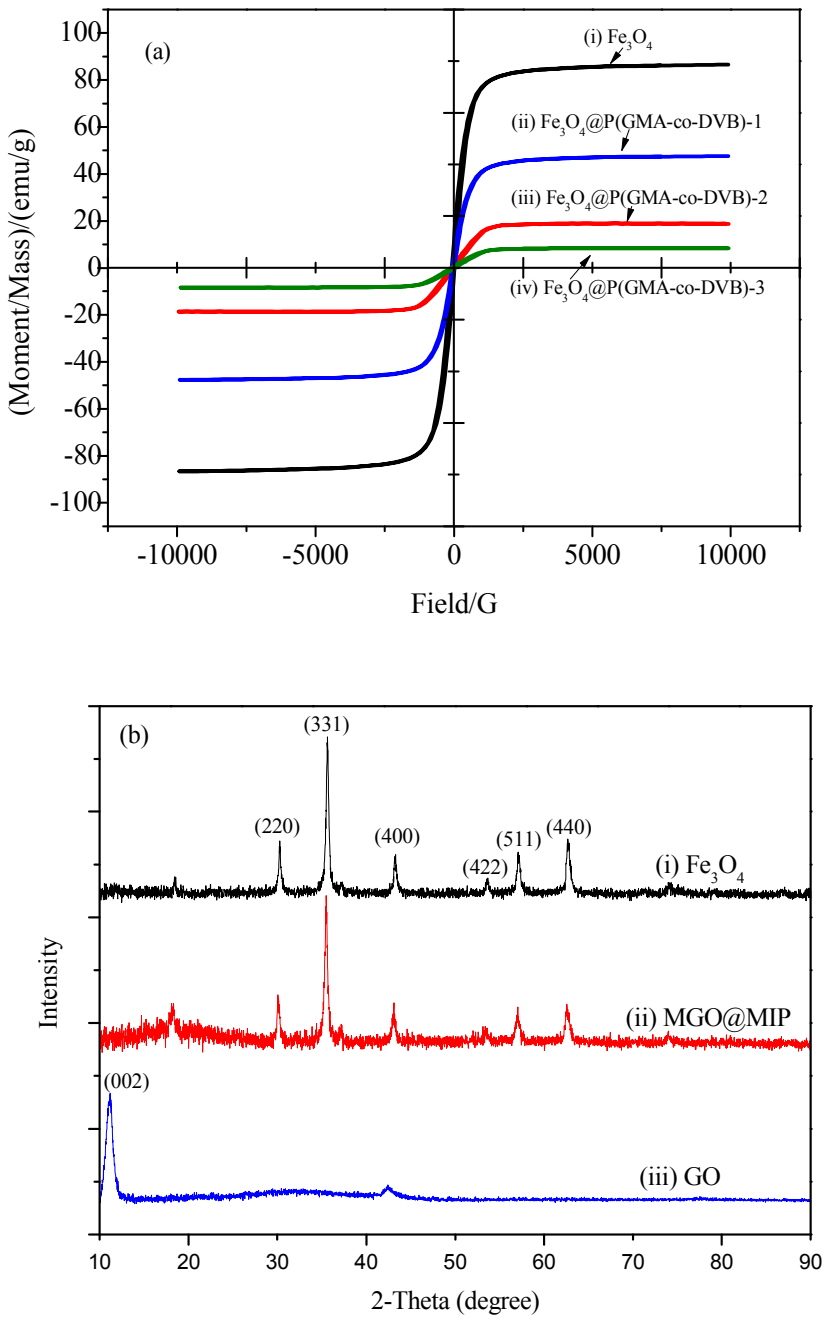

Fig. 2 VSM and XRD characterizations of the as-prepared materials

Journal of Materials Chemistry A Accepted Manuscript

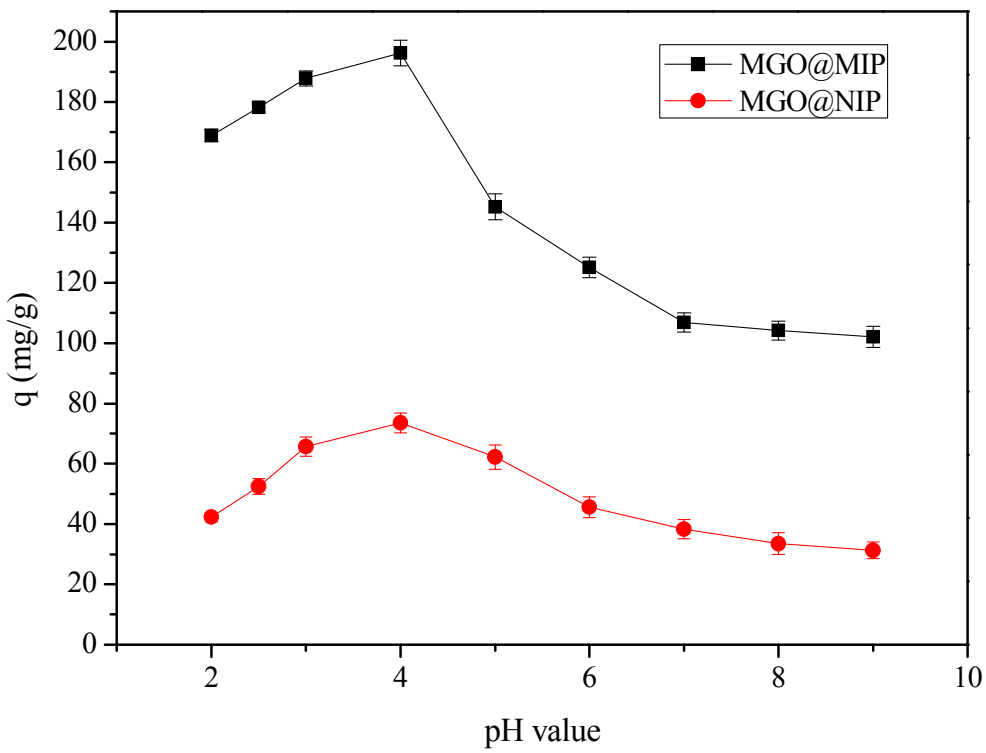

Fig. 3 The pH effect on the PCP adsorption

Journal of Materials Chemistry A Accepted Manuscript

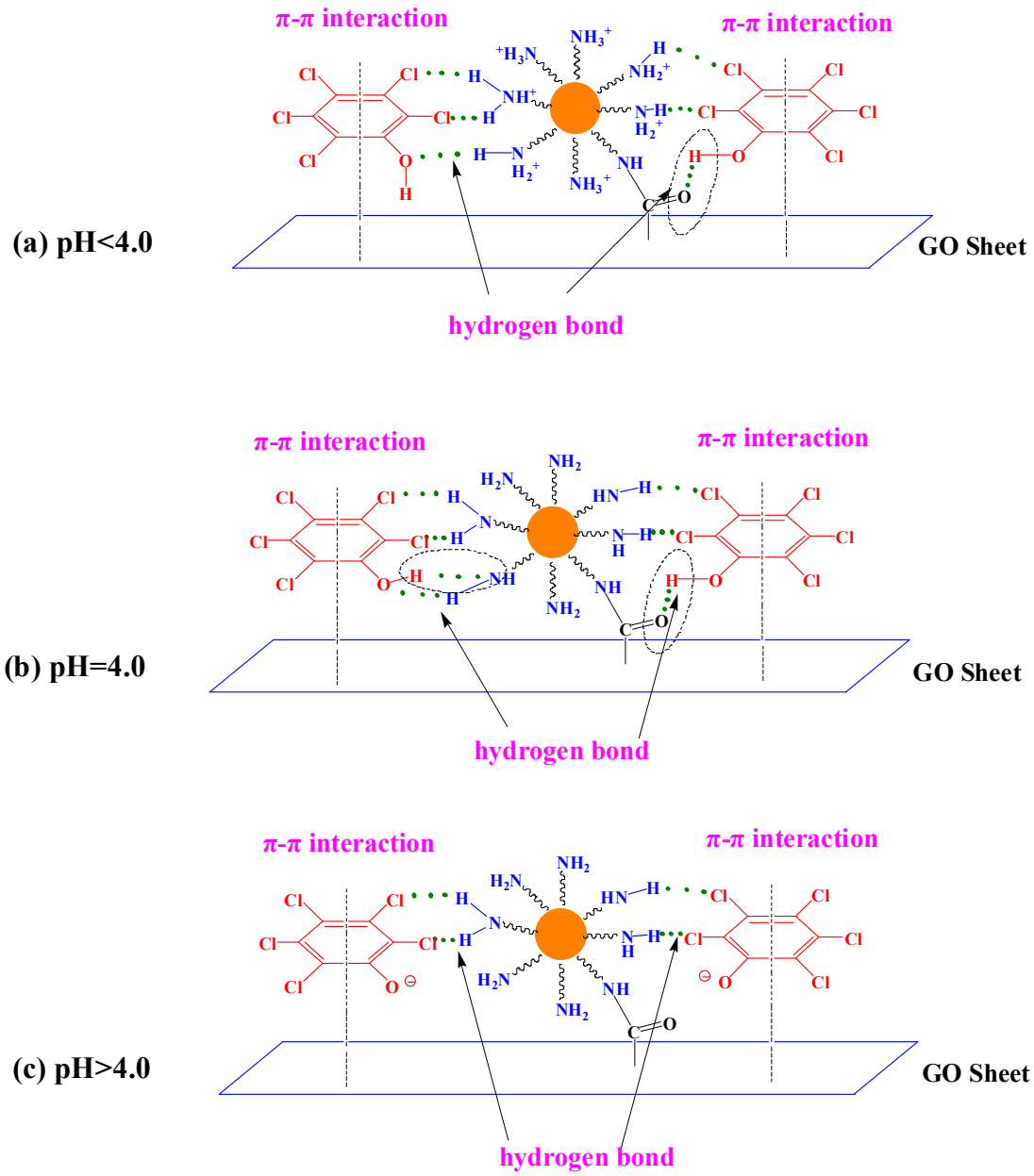

Fig. 4 Probable adsorption mechanism of PCP on the MGO@MIP

Journal of Materials Chemistry A Accepted Manuscript

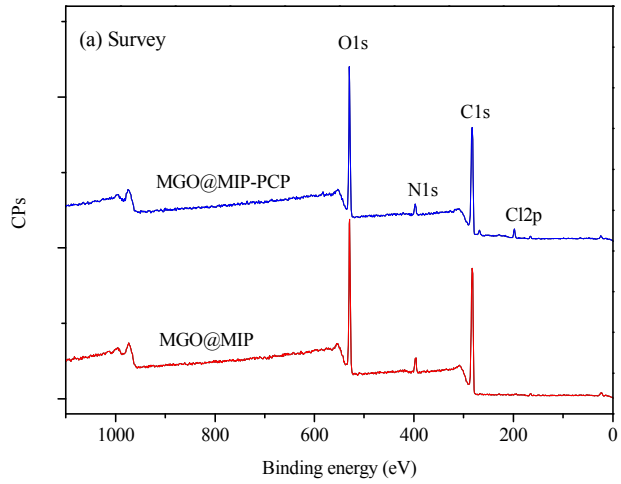

632

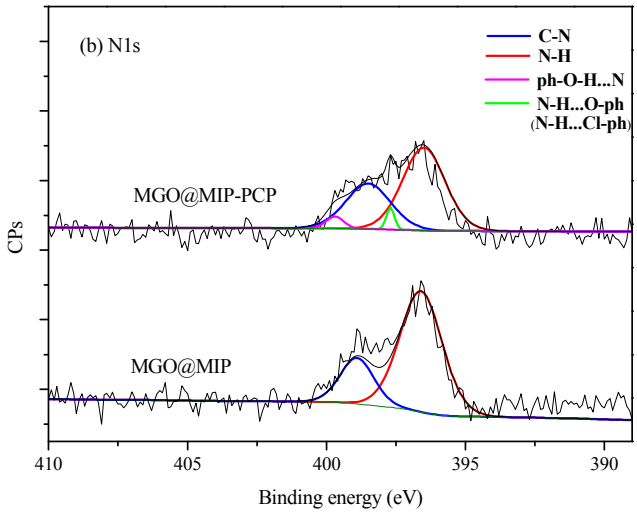

633

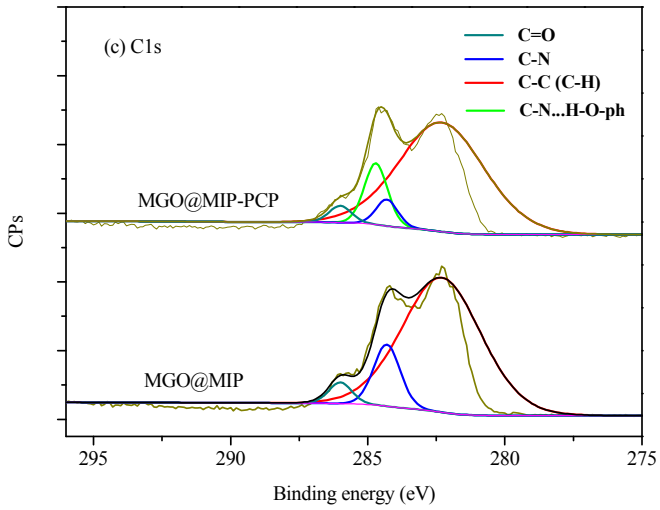

634

Journal of Materials Chemistry A Accepted Manuscript

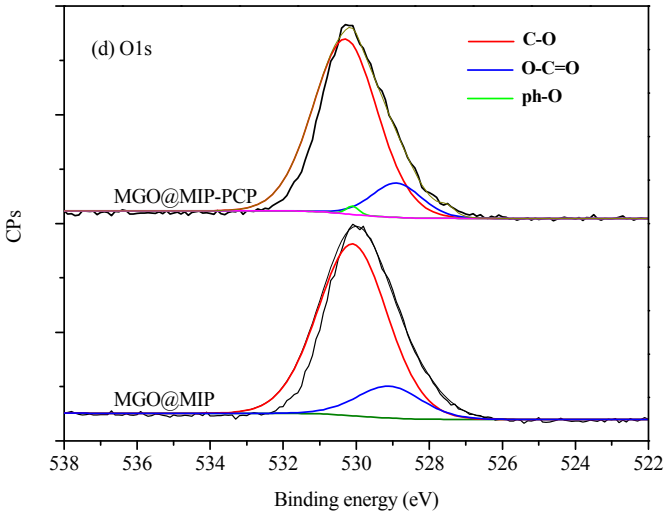

635

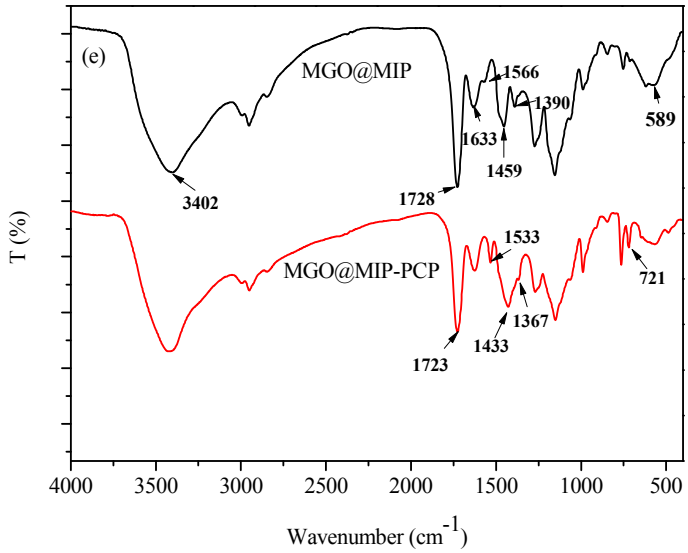

636

Journal of Materials Chemistry A Accepted Manuscript

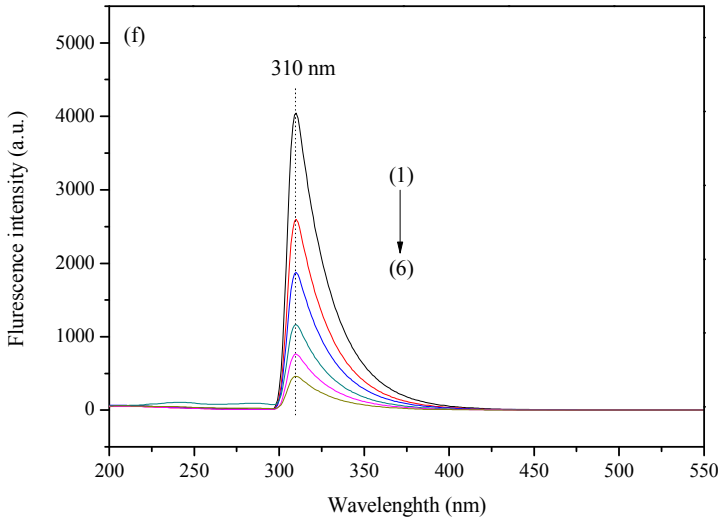

Fig. 5 XPS spectra of (a) survey scan, and high-resolution scan of: (b) N1s; (c) C1s; (d) O1s; (e) FTIR curves of MGO@MIP and MGO@MIP-PCP; (f) fluorescence spectroscopy of: (1) MGO@MIP, (2) PCP, (3)~(6) MGO@MIP adsorbed with different amount of PCP (initial PCP concentrations at 10 mg/L, 100 mg/L, 500 mg/L, and 800 mg/L, respectively).

Journal of Materials Chemistry A Accepted Manuscript

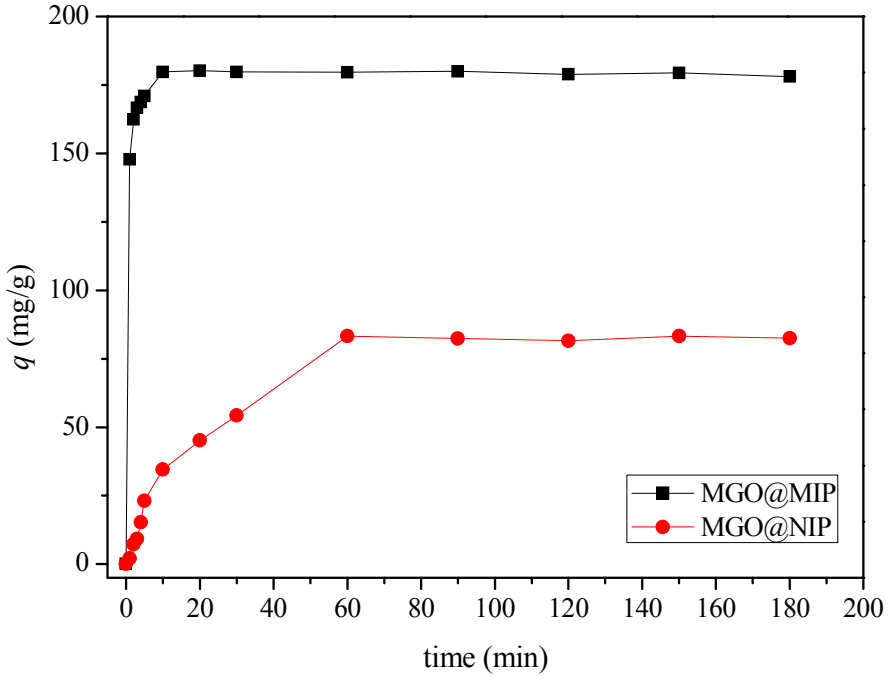

Fig. 6 Effect of adsorption time on the adsorption of PCP onto MGO@MIP and MGO@NIP

Journal of Materials Chemistry A Accepted Manuscript

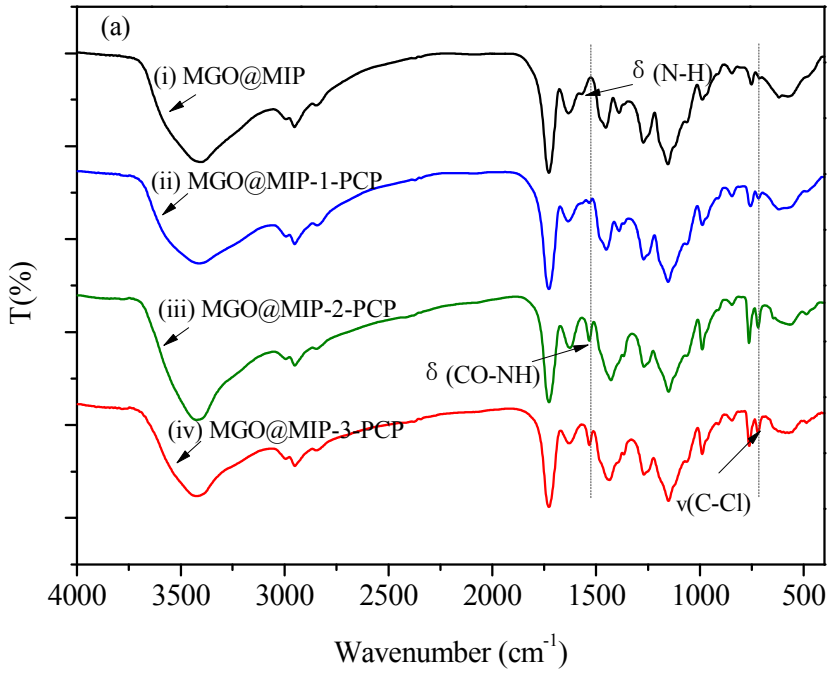

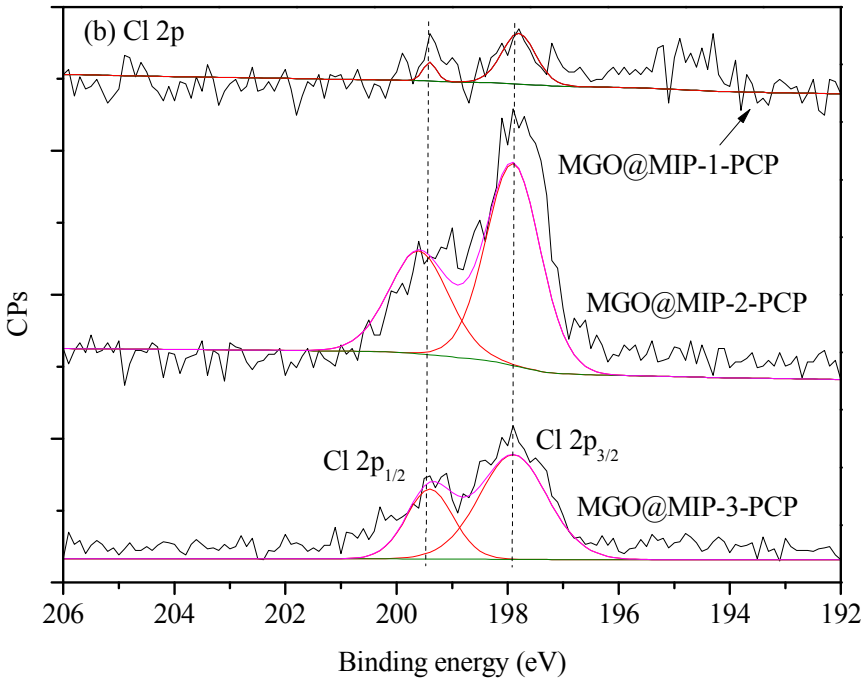

Fig. 7 (a) FTIR and (b) Cl2p high-resolution XPS curves of PCP loaded MGO@MIP with different polymer shell thicknesses

Journal of Materials Chemistry A Accepted Manuscript

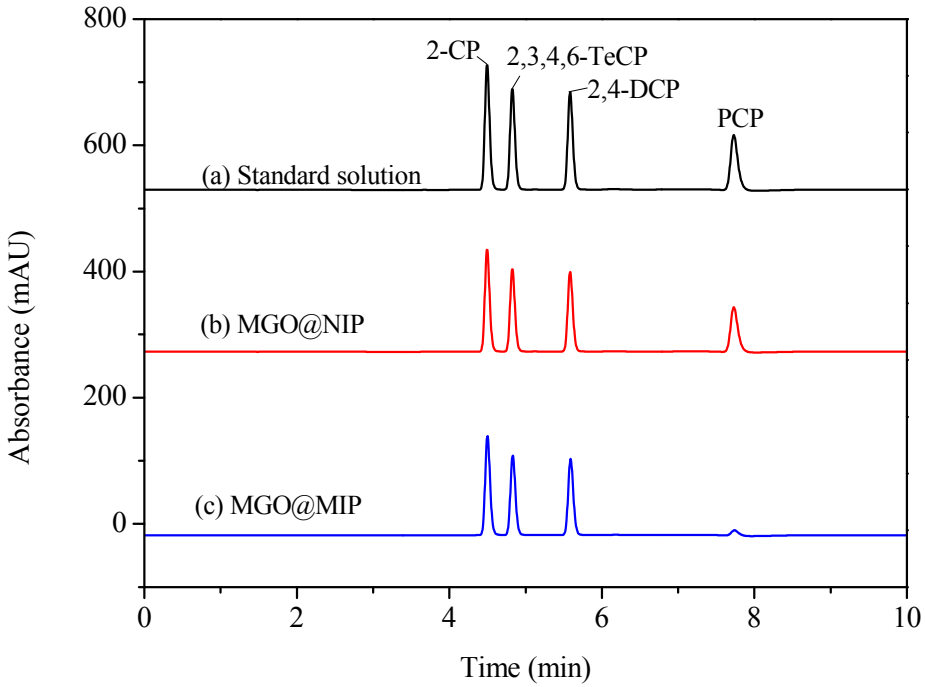

Fig. 8 HPLC chromatograms of (a) standard solution spiked with four CPs at the concentration of 100 mg/L; (b) CPs solution adsorbed by MGO@NIP and (c) CPs solution adsorbed by MGO@MIP, respectively

Journal of Materials Chemistry A Accepted Manuscript

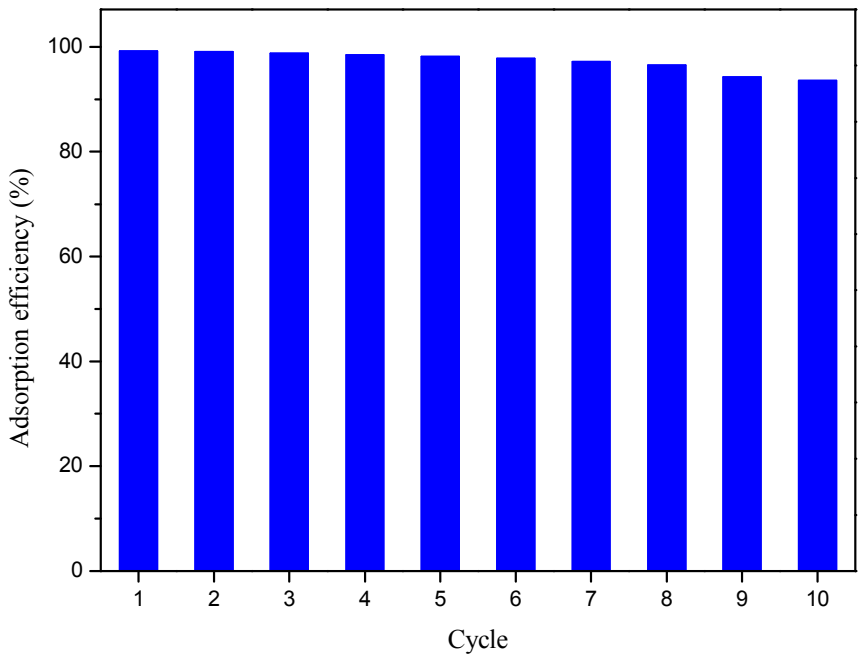

Fig. 9 Adsorption efficiency of PCP on MGO@MIP in ten cycles

Journal of Materials Chemistry A Accepted Manuscript

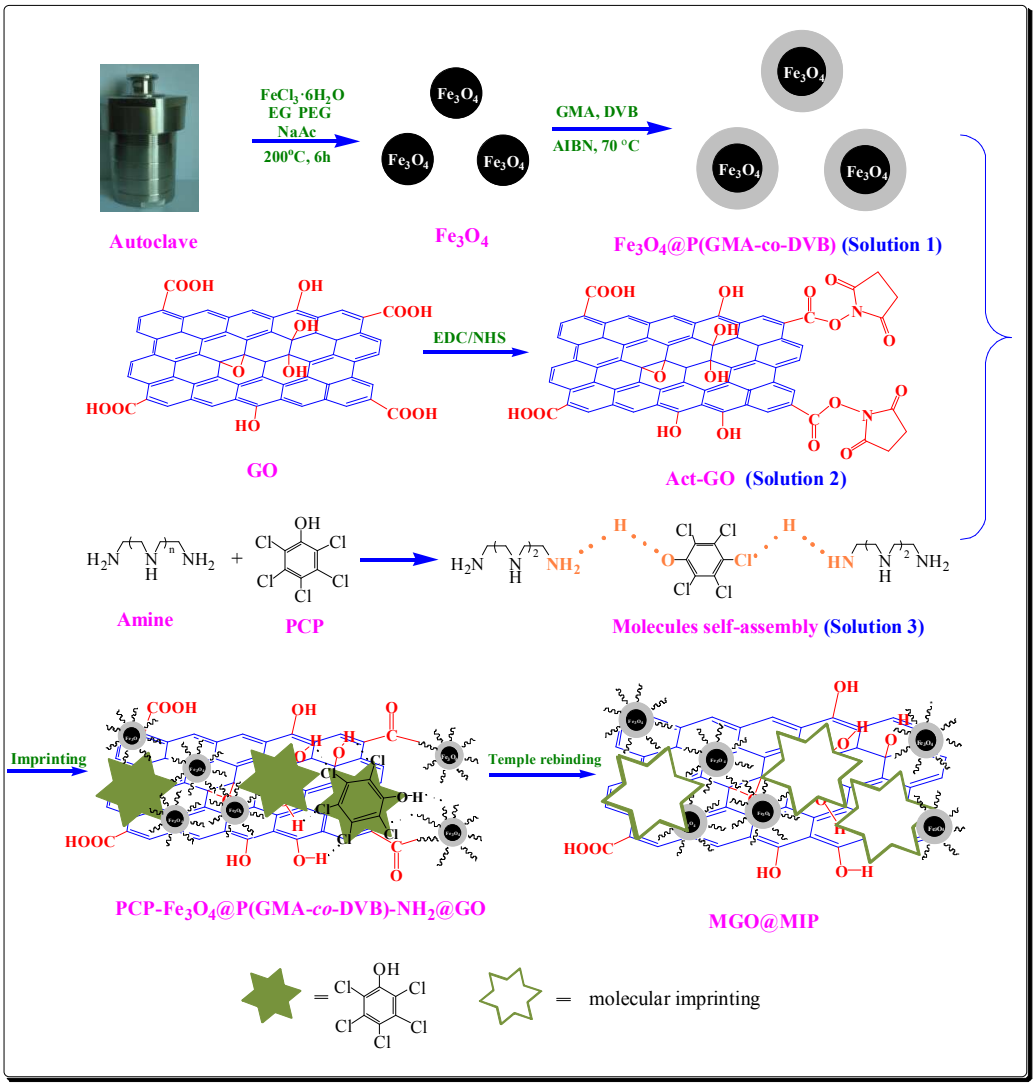

Scheme 1 Schematic procedure of the controllable synthesis of MGO@MIP

Journal of Materials Chemistry A Accepted Manuscript

Table 1 Recipes of core-shell Fe_3O_4@P(GMA-*co*-DVB) microspheres

Samples	GMA (m_1, g)	DVB (m_2, g)	Fe_3O_4 (m_3, g)	(m_1+m_2) /m_3	Shell thickness (nm)	D_n (nm)	D_w (nm)	U
Fe_3O_4@P(GMA-*co*-DVB)-1[b]	0.10	0.10	0.08	2.5	50	400	431	1.08
Fe_3O_4@P(GMA-*co*-DVB)-2[b]	0.60	0.60	0.08	15	310	920	1025	1.11
Fe_3O_4@P(GMA-*co*-DVB)-3[b]	1.12	1.12	0.08	28	520	1340	1613	1.20

[b] Fe_3O_4@P(GMA-*co*-DVB)-1, Fe_3O_4@P(GMA-*co*-DVB)-2 and Fe_3O_4@P(GMA-*co*-DVB)-3 mean the core-shell magnetic polymers with the ratio of the usage amount of monomers (GMA+DVB, GMA:DVB=1:1) to Fe_3O_4 at 2.5, 15 and 28, respectively, during the polymerization process.

Table 2 Pseudo-second-order rate equations and constants of MGO@MIP and MGO@NIP

Adsorbent	equations	k_2 (g/(mg· min))	q_e (mg/g)	$q_{e,cal}$ (mg/g)	R^2
MGO@MIP	t/q_t=0.0056t+0.002	0.157	179.8	178.6	0.9999
MGO@NIP	t/q_t=0.0121t+0.023	0.198	83.3	82.6	0.9995

Table 3 Freundlich istherm equations and corresponding constants

Adsorbents	Freundlich isotherm	Freundlich constants		q_m[c] (mg/L)	R^2
		K_F	n		
MGO@MIP	log q_e=0.4633log C_e+1.6079	40.54	2.158	789.4	0.9998
MGO@NIP	log q_e=0.8921 log C_e+1.3288	21.32	1.121	373.2	0.9993

c q_m obtained at an initial PCP concentration of 1000.0 mg/L.

Journal of Materials Chemistry A Accepted Manuscript

Table 4 Imprinting factors (α) and selectivity factors (β) of MGO@MIP and MGO@NIP

Compounds	q (MGO@MIP) (mg/g)	q (MGO@NIP) (mg/g)	α	β
PCP	175.8	40.3	4.36	
2-CP	38.2	37.6	1.02	4.27
2,4-DCP	36.6	36.2	1.01	4.32
2,3,4,6-TeCP	39.3	38.9	1.01	4.32

Table 5 Comparison with the current adsorbents for PCP removal

Adsorbents	Initial concentration (mg/L)	Sample pH value	Equilibrium Time (min)	Adsorption isotherm[d]	q_m (mg/g)	Ref.
MGO@MIP	10-1000	4.5	10	F	789.4	This work
MGO@NIP	10-1000	4.5	60	F	373.2	This work
chitosan	103.9	6.2	240	L and F	18.7	[8]
organoclays	5.0-250.0	5.0	80	F	7.09	[9]
poly(St-co-DVB) functionalized materials	102-230	6.5	360	F	292.01	[10]
β-cyclodextrin polymer	21.0-150.0	7.0	150	L and F	179.73	[11]
Multiwalled carbon nanotubes (MWCNTs)	0.03-1.2	—	60	Radke-Prausnitz and Fritz-Schlünder models	6	[12]

[d] L, Langmuir isotherm; F, Freundlich isotherm.

Journal of Materials Chemistry A Accepted Manuscript